Structural damage to meiotic chromosomes impairs DNA recombination and checkpoint control in mammalian oocytes

Hong Wang and Christer Höög

Department of Cell and Molecular Biology, Karolinska Institutet, SE-171 77 Stockholm, Sweden

Meiosis in human oocytes is a highly error-prone process with profound effects on germ cell and embryo development. The synaptonemal complex protein 3 (SYCP3) transiently supports the structural organization of the meiotic chromosome axis. Offspring derived from murine *Sycp3*$^{-/-}$ females die in utero as a result of aneuploidy. We studied the nature of the proximal chromosomal defects that give rise to aneuploidy in *Sycp3*$^{-/-}$ oocytes and how these errors evade meiotic quality control mechanisms. We show that DNA double-stranded breaks are inefficiently repaired in *Sycp3*$^{-/-}$ oocytes, thereby generating a temporal spectrum of recombination errors. This is indicated by a strong residual γH2AX labeling retained at late meiotic stages in mutant oocytes and an increased persistence of recombination-related proteins associated with meiotic chromosomes. Although a majority of the mutant oocytes are rapidly eliminated at early postnatal development, a subset with a small number of unfinished crossovers evades the DNA damage checkpoint, resulting in the formation of aneuploid gametes.

Introduction

A quarter of all conceived human embryos are aneuploid, i.e., they either have too many or too few chromosomes (Hassold and Hunt, 2001). The consequences of such chromosomal abnormalities are profound, affecting not only fertility, but also triggering spontaneous miscarriages. A few abnormal karyotypes are compatible with human life, including Down's (trisomy 21), Turner (a single X chromosome), and Klinefelter's (XXY) syndromes, but are also associated with developmental disabilities of variable penetrance. Analysis of human sperm and eggs has revealed that aneuploidy affecting embryos is primarily caused by an error-prone meiotic chromosome segregation mechanism in oocytes. Whereas ∼1–2% of human sperm have an abnormal chromosomal content (the same level of aneuploidy is recorded in mouse haploid germ cells, including oocytes), an astonishing 20–25% of the human oocytes are aneuploid (Hassold and Hunt, 2001). The cause of this high error rate for the meiotic process in human female germ cells is unclear.

Meiosis is a specialized cell division process that generates genetically distinct haploid cells through a process that involves one DNA replication step followed by two cell divisions (Zickler and Kleckner, 1999; Page and Hawley, 2004). The newly replicated sister chromatids are bound by cohesin complex proteins that ensure that cohesion between sister chromatids is retained at the first cell division, but lost at the second meiotic division (Petronczki et al., 2003). Each pair of cohesin-bound sister chromatids constitutes a chromosome, which subsequently becomes connected with its homologous partner at the zygotene to pachytene stages of prophase I in a process called synapsis. The synaptic process is promoted by the formation of a large number of DNA double-stranded breaks (DSBs) that are generated by the topoisomerase II–related transesterase SPO11 (Gerton and Hawley, 2005). The repair of a subset of the DSBs results in crossovers between the homologous chromosomes and, ultimately, in chiasmata, providing essential physical links between the chromosomes (Zickler and Kleckner, 1999; Gerton and Hawley, 2005; Marcon and Moens, 2005). Synapsis is also dependent on a conserved proteinaceous structure called the synaptonemal complex (SC). The SC is composed of two axial elements (AEs) and a large number of individual transverse filaments that connect the AEs along their entire length. In addition, a central element has been defined at

the center of the transverse filament structure (Zickler and Kleckner, 1999; Page and Hawley, 2004). In mammalian male and female germ cells, several different meiosis-specific proteins have been defined as components of the SC, including the AE proteins SC protein 2 (SYCP2) and 3 (Dobson et al., 1994; Lammers et al., 1994; Schalk et al., 1998) and the transverse filament protein SYCP1 (de Vries et al., 2005). The AE proteins SYCP2 and -3 are found at the interchromatid domains of the sister chromatids, which is where they jointly form axial cores together with the cohesin complex proteins.

Several different error surveillance systems (checkpoints) have been characterized in meiotic cells (Lydall et al., 1996; Roeder and Bailis, 2000; Di Giacomo et al., 2005). A failure to repair DSBs that is caused by inactivation of DNA repair/recombination proteins such as DMC1, MSH4, and MSH5, or DNA damage checkpoint proteins such as ATM, will activate a DNA damage checkpoint that results in female germ cell death at early postnatal development (Di Giacomo et al., 2005). The mismatch repair protein MLH1 takes part in the conversion of crossovers into chiasmata at a late stage of the recombination pathway (Baker et al., 1996; Edelmann et al., 1996; Hunter and Borts, 1997). Surprisingly, inactivation of this protein in murine germ cells does not activate a DNA damage checkpoint. Instead, in mouse oocytes that are deficient for *Mlh1*, the resulting achiasmatic mutant germ cells cannot establish a proper meiotic spindle and are eliminated at the metaphase I stage by the spindle checkpoint (Woods et al., 1999).

The absence of SYCP3 results in decompaction of the meiotic chromosome axis, premature loss of cohesin complexes from the meiotic chromosome axis, and irregular interruptions of the synaptic process as defined by SYCP1 (Yuan et al., 2002; Kouznetsova et al., 2005). Female *Sycp3*$^{-/-}$ mice are fertile, although one-third of their offspring die in utero at an early stage of embryonic development as a result of aneuploidy (Yuan et al., 2002). We investigated the nature of the chromosomal

errors introduced by the absence of SYCP3 and how these errors evade the meiotic quality assurance systems, thereby generating aneuploid offspring. Our results illustrate the importance of the axial element of the synaptonemal complex for efficient repair of recombination events.

Results

Loss of SYCP3 affects germ cell cyst survival and primordial follicle formation

The absence of SYCP3 results in a complete elimination of male spermatocytes at the zygotene–pachytene transition of prophase I (Yuan et al., 2000). To investigate how the elimination of SYCP3 affects the oocyte maturation process, ovarian morphology and oocyte numbers were analyzed in pre- and postnatal animals from embryonic day (E) 16.5 to 8 d postpartum (dpp). Sequential sections of ovaries taken from wild-type or *Sycp3*$^{-/-}$ animals were either stained with hematoxylin and eosin or immunostained using antibodies against germ cell nuclear antigen (GCNA) or c-kit. GCNA and c-kit specifically stain the nuclei and the cytoplasm of oocytes, respectively (Manova et al., 1990; Enders and May, 1994). Histomorphometric analysis revealed no difference in the relative numbers of oocytes at E16.5, E18.5, or at birth when ovaries from wild-type or *Sycp3*$^{-/-}$ females were compared (Fig. 1 A and Fig. 2 A). This shows that germ cell development is not interrupted before the diplotene stage in *Sycp3*$^{-/-}$ females. A majority of the oocytes in 1-dpp mice are found in small clusters, called germ cell cysts, which are seen in both wild-type and mutant ovaries (Fig. 1, A and B). Starting at 2 dpp, we noted a distinct loss of germ cell cysts in the *Sycp3*$^{-/-}$ ovary, which was not seen in the wild-type ovary (Fig. 1, C and D, and Fig. 2 B). The relative loss of germ cell cysts in the *Sycp3*$^{-/-}$ ovary was further accentuated 4 dpp (Fig. 1, E and F; and Fig. 2 C). We also noted a reduction in the number of primordial oocytes in *Sycp3*$^{-/-}$ ovaries in 2- and 4-dpp mice,

Figure 1. ***Sycp3*$^{-/-}$ oocytes are rapidly and selectively lost after birth.** Oocytes were detected in ovary sections by anti-GCNA1 (A–F) and anti–c-kit (G and H) immunohistochemistry (brown stain). At 1 dpp, both germ cell cysts (arrowhead) and primordial follicles were found in wild-type (A), as well as in *Sycp3*$^{-/-}$ ovaries (B) in a similar number. The inset in B indicates germ cell cysts. (C) At 2 dpp, germ cell cysts (arrowhead) and primordial follicles were detected mostly in the periphery in wild-type. (D) A significant loss of germ cell cysts (arrowhead) and primordial follicles (inset) were observed in the *Sycp3*$^{-/-}$ ovary at 2 dpp. At 4 dpp, both primordial follicles (arrowhead) and primary follicles were detected in wild type (E). A further loss of primordial follicles (arrowhead) was found in the *Sycp3*$^{-/-}$ ovary (F), but no significant difference in the numbers of primary follicles (inset) was detected between wild type and mutant (F). (G and H) At 8 dpp, primordial (arrowheads), primary, and secondary follicles (inset) were detected in wild-type (G) and the *Sycp3*$^{-/-}$ ovaries (H), but the number of primordial follicles was further reduced in the *Sycp3*$^{-/-}$ ovary. Bars, 30 μm.
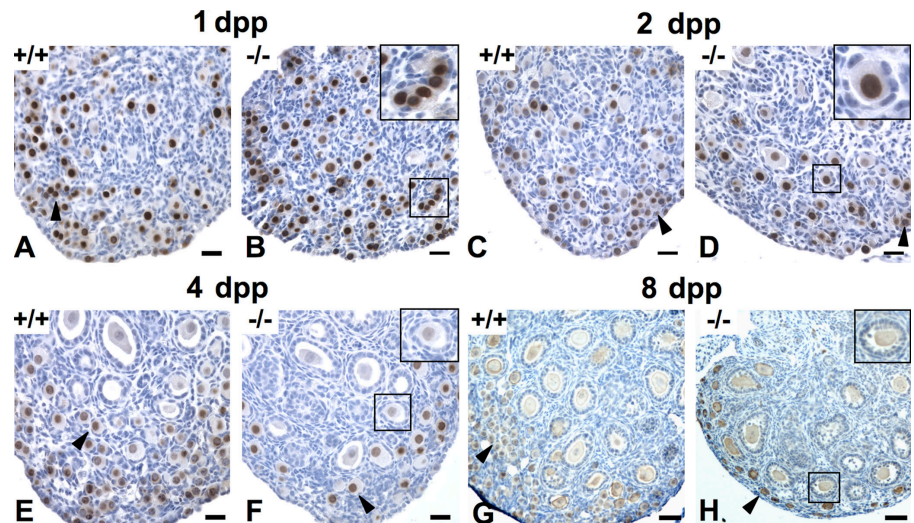
compared with wild type (Fig. 1 and Fig. 2, B and C). It is likely that the loss of primordial oocytes is attributable to the rapid elimination of the germ cell cysts seen during early postnatal development, as the primordial oocytes develop from these cysts. We found that the collective loss of germ cell cysts and primordial oocytes in the mutant ovary amounts to 34% in 2-dpp mice and 52% in 4-dpp mice (Fig. 2 A). A further reduction in primordial follicle number occurs at 8 dpp (Fig. 1 and Fig. 2 D), suggesting that primordial follicles are also susceptible to elimination within the mutant ovary environment. Notably, however, the residual fraction of primordial follicles in the $Sycp3^{-/-}$ ovary gives rise to both primary and secondary follicles in numbers that closely match the wild-type situation. We conclude that loss of SYCP3 function results in a drastic loss of germ cell cysts and primordial follicles during early postnatal development. The oocyte pool established 8 dpp in $Sycp3^{-/-}$ females is reduced, with ∼66% compared with wild-type, but no further depletion occurs relative to wild type, giving rise to an oocyte reservoir in 8–12-wk-old $Sycp3^{-/-}$ females that can sustain normal levels of fertility at this age (Yuan et al., 2002).

The loss of germ cell cysts and primordial follicles in the ovary of the mutant females could be caused by an apoptotic process that is introduced by the absence of SYCP3. TUNEL staining showed an increase in the number of apoptotic cells at 1 and 2 dpp in the $Sycp3^{-/-}$ ovary, compared with the wild-type counterpart (Fig. S1, available at http://www.jcb.org/cgi/content/full/jcb.200512077/DC1). The ovarian cells labeled by TUNEL staining in the $Sycp3^{-/-}$ females are predominantly localized at the cortex area (at the outer edge of the ovary sections), suggesting that the affected cells correspond to the germ cell cysts that are preferentially lost in the mutant background. The number of TUNEL-positive cells is low, relative to the total number of oocytes that are lost in the mutant ovary. This is most likely because of the transient nature of the TUNEL staining, which is also described in another mouse model monitoring female germ cell death during early postnatal development (Rajkovic et al., 2004).

Absence of SYCP3 affects the efficiency of the DSB repair process in meiotic cells

The temporal profile of the oocyte loss in $Sycp3^{-/-}$ females suggests the involvement of the DNA damage checkpoint, which is known to become active at an early stage of postnatal development in oocytes (Di Giacomo et al., 2005). Therefore, we monitored the progression of DNA repair of DSBs in zygotene to diplotene mutant oocytes. The principles used to define the different meiotic stages in $Sycp^{-/-}$ oocytes are described in Fig. S1, Materials and methods, and Kouznetsova et al. (2005). In brief, both early zygotene and zygotene oocytes were derived from E16.5 embryos, whereas pachytene and diplotene oocytes were derived from E18.5 or E19.5 embryos. Formation of the axial cores was monitored by STAG3 staining, synapsis (transverse filament formation) was monitored by SYCP1 staining, and centromere morphology was monitored by CREST staining. Introduction of DSBs in meiotic DNA at the leptotene stage of prophase I results in the phosphorylation of H2AX (generating a modified form called γH2AX). γH2AX appears at leptotene in chromatin regions throughout the nucleus and generally form large, cloud-like patterns, suggesting that the majority of the affected H2AX molecules are found in chromatin loops that project out from the axial cores of the chromosomes (Mahadevaiah et al., 2001; Celeste et al., 2002). Subsequent repair of DSBs results in the disappearance of most of the γH2AX signal at the pachytene stage. A second and independent wave of γH2AX staining appears in late zygotene and pachytene cells, which are associated specifically with the asynapsed axial cores of the meiotic chromosomes (de Vries et al., 2005; Turner et al., 2005). We found that γH2AX immunostaining of wild-type early zygotene oocytes revealed dispersed, cloud-like signals throughout the nucleus (Fig. 3, C and D), whereas only a few patches of γH2AX signals associated with the remaining asynaptic axial cores were observed in pachytene nuclei (Fig. 3, G and H). We also consistently observed a few residual γH2AX patches in diplotene nuclei, the nature of which is not clear (Fig. 3, K and L). We then analyzed the distribution of γH2AX
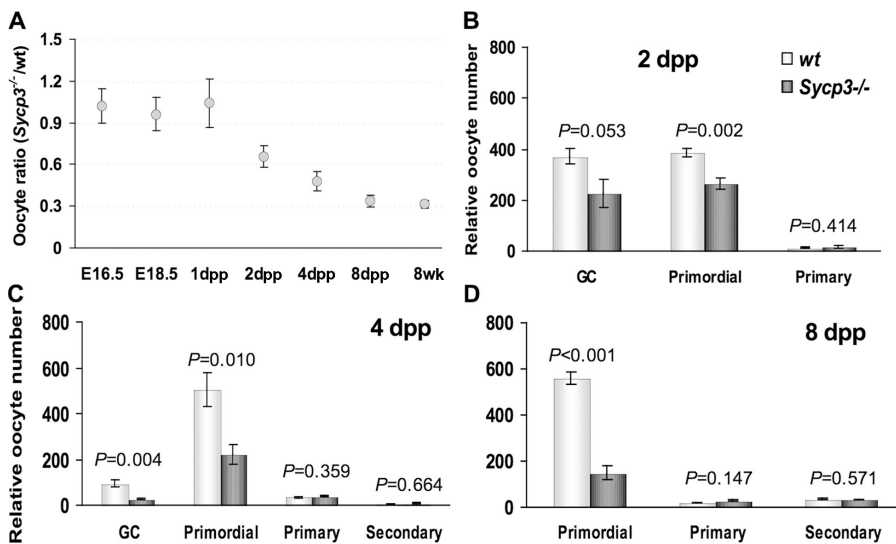
Figure 2. **Germ cell cysts and primordial follicles are preferentially lost in the $Sycp3^{-/-}$ ovary.** (A) The ratio of $Sycp3^{-/-}$/wild-type (wt) oocytes indicates no difference in the relative numbers found in wild-type and $Sycp3^{-/-}$ ovaries at E16.5 (n = 4), E18.5 (n = 3), or at birth (1 dpp; n = 5). The oocyte number in $Sycp3^{-/-}$ ovary was reduced by ∼34% at 2 dpp (n = 5), ∼52% at 4 dpp (n = 5), and ∼66% at 8 dpp (n = 7), as compared with wild-type. No further reduction was detected in $Sycp3^{-/-}$ ovary at 8 wk (68%; n = 4). A significant reduction of germ cell cysts and primordial follicles were observed in the $Sycp3^{-/-}$ ovary at 2 (B) and 4 dpp (C), whereas a large fraction of the primordial follicles in $Sycp3^{-/-}$ ovaries were lost at 8 dpp (D). The numbers of the primary and secondary follicles remain the same in both wild-type and mutant ovaries during early follicle development at 2 (B), 4 (C), and 8 dpp (D). Values shown represent the mean ± SEM. Statistical analysis was performed by one-way analysis of variance, and significance was shown in p-values.

Figure 3. **Absence of SYCP3 strongly affects γH2AX distribution during meiotic prophase development.** (A–D) γH2AX (green) staining is abundantly distributed throughout the nucleus in early zygotene wild-type and *Sycp3⁻/⁻* oocytes. Synapsed regions are labeled by SYCP1 (red) and centromeres (white) are visualized by CREST. (G and H) Only a few γH2AX patches remain in pachytene wild-type oocytes. The γH2AX staining is associated with the SYCP1-labeled structures of the SC and protrudes from these structures. (E and F) Pachytene *Sycp3⁻/⁻* oocytes retain a strong and ubiquitously distributed γH2AX staining pattern. (K and L) A few residual γH2AX patches were detected in diplotene wild-type oocytes. (I and J) Strong γH2AX staining similar to the pattern seen in early zygotene and pachytene oocytes is retained in diplotene *Sycp3⁻/⁻* oocytes. Bar, 10 μm.
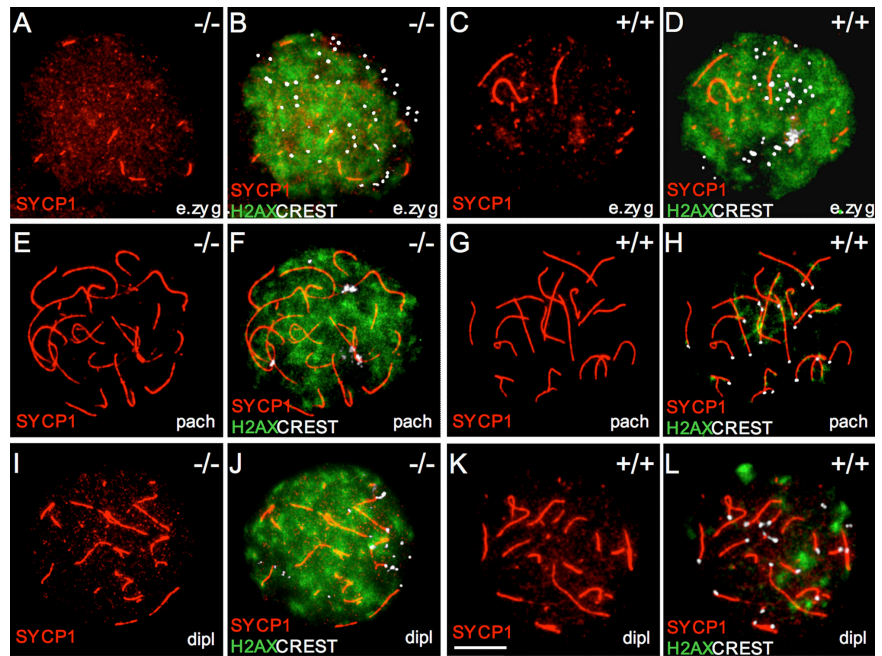
in *Sycp3⁻/⁻* oocytes at the early zygotene stage and noted that it was indistinguishable from the pattern observed in wild-type cells at this stage (Fig. 3, A and B). This suggests that neither SPO11-derived DSB formation nor phosphorylation of H2AX is dependent on SYCP3 expression. Surprisingly, however, analysis of pachytene and diplotene *Sycp3⁻/⁻* oocytes revealed that a majority of these cells retained a strong, cloud-like nuclear γH2AX signal, which is similar to the pattern seen in early zygotene cells (Fig. 3, E, F, I, and J). Strong γH2AX staining in late meiotic cells could reflect inefficient DNA repair or residual asynapsis. The nuclear distribution of the γH2AX pattern seen in pachytene and diplotene *Sycp3⁻/⁻* oocytes, however, is very different from the γH2AX pattern seen in meiotic cells with asynapsed chromosomes (de Vries et al., 2005; Turner et al., 2005). Our results show that SYCP3 is required for efficient dephosphorylation of γH2AX during meiosis, and the nuclear pattern displayed by this marker in pachytene and diplotene *Sycp3⁻/⁻* oocytes suggests that the DNA repair process is impaired in the mutant cells.

Absence of SYCP3 affects the turnover of recombination-related proteins

To monitor if the meiotic repair/recombination process is affected in *Sycp3⁻/⁻* oocytes, the spatial and temporal distribution of several DNA repair/recombination proteins were studied during meiosis. The RecA homologues RAD51 and DMC1 take part in heteroduplex formation during meiosis (Shinohara and Shinohara, 2004). RAD51 and DMC1 foci are formed along the AEs in wild-type meiotic cells and are observed on both asynapsed and synapsed parts of the SC, but these foci disappear during pachytene (Moens et al., 2002). We observed a similar number of RAD51/DMC1 foci at the early zygotene and zygotene stages in *Sycp3⁻/⁻* oocytes, as seen in wild-type cells (Fig. 4, A, C, and D). However, as meiosis progressed, an increased

number of foci were retained in *Sycp3⁻/⁻* pachytene and diplotene oocytes, compared with wild-type cells (Fig. 4, G, H, K, and L). Most of the persistent RAD51/DMC1 foci in *Sycp3⁻/⁻* oocytes were found in the nuclear space next to the SCs (labeled by SYCP1), but an increased number of foci associated with the SC were also seen (Fig. S2, available at http://www.jcb.org/cgi/content/full/jcb.200512077/DC1). RPA is a single-stranded DNA–binding protein that promotes DNA DSB repair (Alani et al., 1992; Wang and Haber, 2004). RPA foci appear on the SCs later than RAD51/DMC1 foci and have been suggested to be part of an antirecombination protein complex that prevents the formation of superfluous reciprocal recombination events (Moens et al., 2002). We found that the number of RPA foci at early zygotene, zygotene, and late zygotene was similar in wild-type and *Sycp3⁻/⁻* oocytes (Fig. 4, B, E, and F). Starting at pachytene, however, the number of RPA foci observed in *Sycp3⁻/⁻* oocytes did not decrease, as in wild-type oocytes at this stage (Fig. 4, I and J). Furthermore, many RPA foci remained in *Sycp3⁻/⁻* diplotene oocytes, despite an almost complete loss of such foci in wild-type oocytes at the same stage (Fig. 4, M and N). MSH4 is a MutS homologue that promotes homologous alignment and crossover formation (Neyton et al., 2004). MSH4 foci overlap with RPA foci, but appear slightly later during meiosis in mouse germ cells (Moens et al., 2002). We found that an increased number of MSH4 foci persist at late meiotic stages in *Sycp3⁻/⁻* oocytes (unpublished data).

Finally, we monitored the expression of the DNA mismatch repair protein MLH1 in *Sycp3⁻/⁻* oocytes. MLH identifies the sites of meiotic exchanges along the pachytene chromosomes and is critical for chiasma formation (Baker et al., 1996; Edelmann et al., 1996; Hunter and Borts, 1997; Anderson et al., 1999). It has been shown that the number of MLH1 foci varies according to the length of the SC (Lynn et al., 2002). This correlation, however, does not apply to SYCP3-deficient meiotic
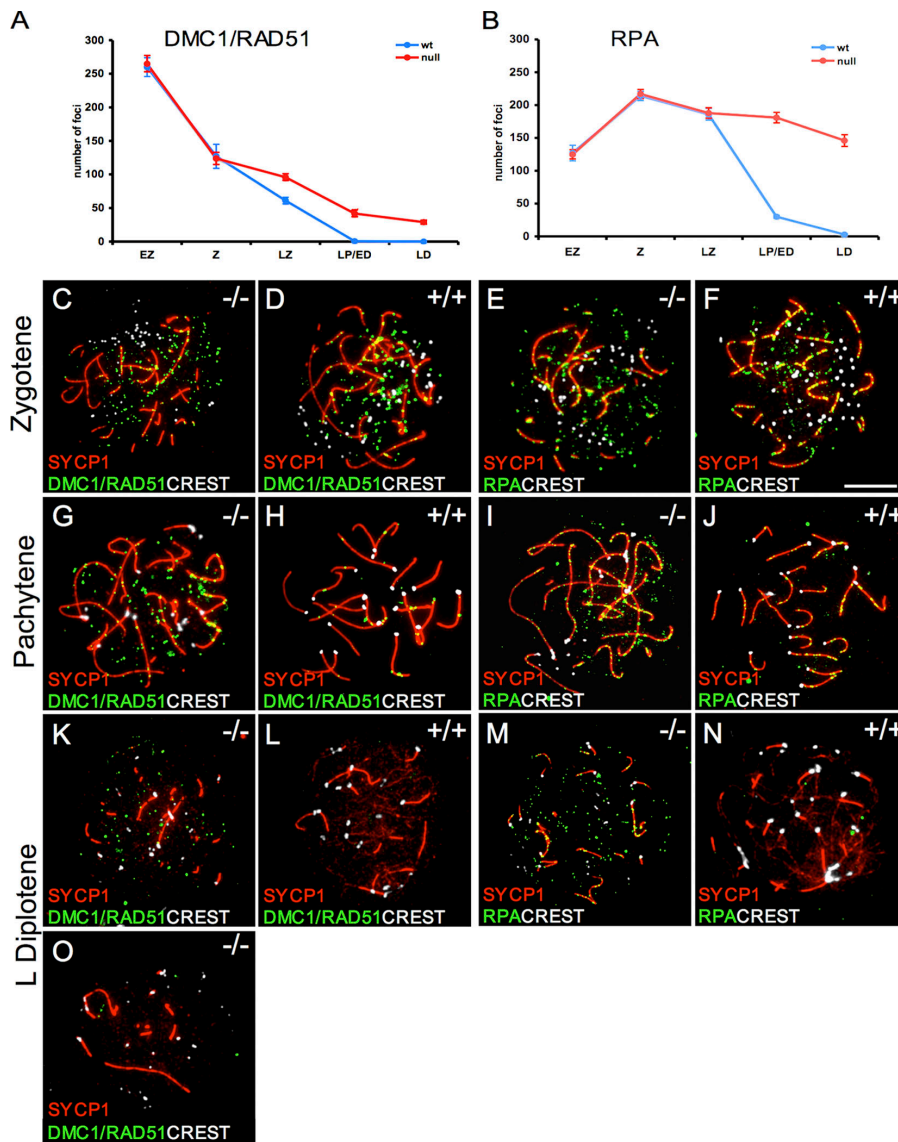
Figure 4. **Absence of SYCP3 affects the turnover of DMC1/RAD51 and RPA foci during meiosis.** (A and B) The number of RAD51/DMC1 and RPA foci was presented as the mean ± SEM of analyzed oocytes from five meiotic stages (n_a, counted wild-type oocytes; n_b, counted $Sycp3^{-/-}$ oocytes). (A) The number of RAD51/DMC1 foci (green) shows no difference between wild-type and $Sycp3^{-/-}$ oocytes at the early zygotene ($n_{ab} = 11$) and the zygotene stages (C and D; $n_a = 12$; $n_b = 19$). Excessive RAD51/DMC1 foci were retained in late zygotene to late diplotene $Sycp3^{-/-}$ oocytes, whereas this number rapidly decreased in wild-type oocytes (G and H and K and L; LZ, $n_a = 30$ and $n_b = 38$; LP/ED, $n_a = 16$ and $n_b = 20$; LD, $n_a = 14$ and $n_b = 38$). However, a subset of the $Sycp3^{-/-}$ oocytes displays fewer foci than the rest (a late diplotene stage oocytes is shown as an example in O). (B) The number of RPA foci (green) is similar in wild-type and $Sycp3^{-/-}$ oocytes at the early zygotene ($n_a = 11$; $n_b = 13$), zygotene (E and F; $n_a = 11$; $n_b = 12$), and late zygotene stages ($n_{ab} = 14$). The RPA foci number remained high in $Sycp3^{-/-}$ oocytes from pachytene until the late diplotene stage, whereas this number sharply decreased in wild-type oocytes (I and J and M and N; LP/ED, $n_a = 43$ and $n_b = 30$; LD, $n_a = 13$ and $n_b = 32$). Synapsed regions were labeled by SYCP1 antibodies (red) and centromeres were visualized by CREST (white). Bars, 10 μm.

chromosomes. Despite a twofold increase in axial core length, approximately the same amount of MLH1 foci are observed in both wild-type and $Sycp3^{-/-}$ pachytene oocytes (Yuan et al., 2002). We have monitored the abundance of MLH1 foci in wild-type and $Sycp3^{-/-}$ oocytes at postpachytene meiotic stages to reveal if the temporal distribution of this protein is affected in the absence of SYCP3. We found that MLH1 foci persisted into the diplotene stage in wild-type oocytes, as previously described (Moens et al., 2002), but that these MLH1 foci disappeared at the end of diplotene (Fig. 5, C and D, G and H, and K and L). In contrast to this, we found that a considerably larger number of MLH1 foci persisted into the late diplotene stage in $Sycp3^{-/-}$ oocytes, and that many of these foci also remained until the very late diplotene stage (Fig. 5, A and B, E and F, and I and J). No MLH1 foci were observed in oocytes after birth (unpublished data). Many of the residual MLH1 foci that were retained at the very late diplotene stage were not associated with SYCP1 staining (Fig. 5, E and I). The most likely explanation for this is that the time course of the desynaptic process (i.e., the removal of SYCP1)

is not affected in mutant oocytes (Fig. 5), whereas MLH1 foci persist for longer in these cells. The residual MLH1 foci, however, remain in association with the meiotic chromosome axis, as shown by the association of these foci with STAG3-staining regions in late diplotene mutant oocytes (Fig. 5, O and P). We noted that mutant oocytes that retained a large number of residual MLH1 foci also displayed a strong nuclear γH2AX staining (Fig. 5, F and J), suggesting that the impaired repair process affects DNA associated with the chromosome axis, as well as with DNA loops that project out from this axis. In summary, we found that the absence of SYCP3 results in a persistent γH2AX pattern during meiotic prophase and in a delayed removal of RAD51/DMC1, RPA, MSH4, and MLH1 from meiotic chromosomes. We conclude that the recombination process is impaired in $Sycp3^{-/-}$ oocytes.

Analysis of $Sycp3^{-/-}$ oocytes at different stages of meiosis, using antibodies that detect γH2AX, RAD51/DMC1, RPA, MSH4, and MLH1, consistently identified two groups of cells, where one group retained less staining than the other (Table I).

Figure 5. Absence of SYCP3 delays the removal of MLH1 during meiosis. The distribution of MLH1 foci (white) and association with synapsed regions (labeled by SYCP1; red) at different stages of meiosis are shown for $Sycp3^{-/-}$ oocytes (C, G, K, and M), whereas wild-type oocytes are shown as a control (A, E, and I). γH2AX (green) and centromeres visualized by CREST (blue) were added to these pictures for $Sycp3^{-/-}$ oocytes (D, H, L, and N) and wild-type oocytes (B, F, and J). A subset of the $Sycp3^{-/-}$ oocytes displays fewer foci than the rest (a very late diplotene stage oocytes is shown as an example [M and N]). A majority of the MLH1 foci in late diplotene $Sycp3^{-/-}$ oocytes was not associated with SYCP1 staining (O, arrows), but was associated with the asynapsed axial cores as defined by the cohesin complex protein STAG3 (P, arrows). (Q) The number of MLH1 foci was presented as the mean ± SEM of analyzed oocytes from five meiotic stages (n_a, counted wild-type oocytes; n_b, counted $Sycp3^{-/-}$ oocytes). The number of MLH1 foci shows no difference between wild-type and $Sycp3^{-/-}$ oocytes at the pachytene (middle to late; A and C; $n_a = 50$; $n_b = 35$) and early ($n_a = 36$; $n_b = 41$) to middle diplotene ($n_a = 24$; $n_b = 29$). An increased number of MLH1 foci relative to wild-type is seen in late (G) and very late diplotene (K) $Sycp3^{-/-}$ oocytes, (LD, $n_a = 20$ and $n_b = 42$; VLD, $n_a = 20$ and $n_b = 24$). Bars, 10 μm.
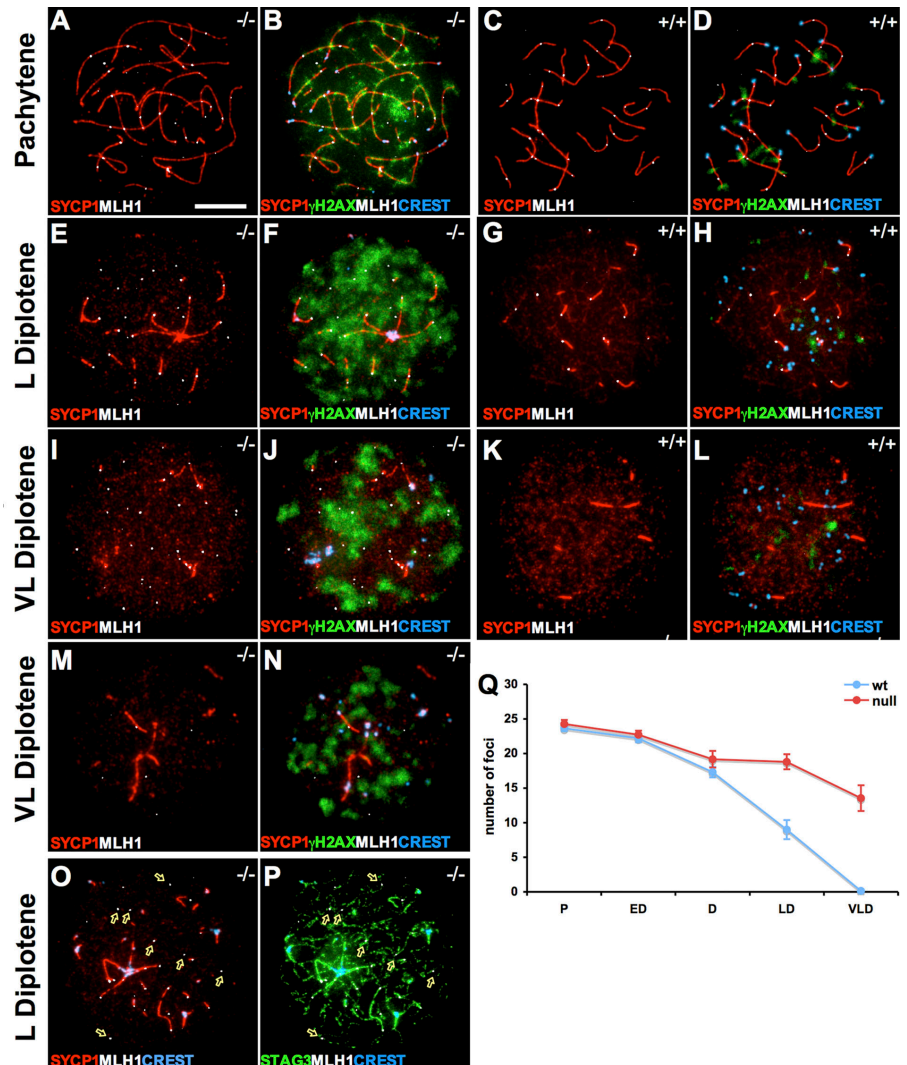
For example, ~29% of the $Sycp3^{-/-}$ late diplotene oocytes displayed weak γH2AX staining. Furthermore, the same percentage of $Sycp3^{-/-}$ oocytes at late diplotene also contained relatively few RAD51/DMC1 and MLH1 foci (Table I, Fig. 4 O, and Fig. 5, M and N). Although the division of the oocytes into two groups is clearly arbitrary, it shows that the repair/recombination process in $Sycp3^{-/-}$ oocytes is impaired, not blocked, giving rise to a spectrum of mutant cells with different levels of damage.

$Sycp3^{-/-}$ ovaries at 2 dpp display a striking increase in oocytes that contain univalent chromosomes

A decreased efficiency of the DNA repair/recombination process should have consequences for completion of the crossing-over process between the homologous chromosomes. A failure to form or maintain chiasmata between the homologous chromosomes during meiosis will result in premature chromosome separation, giving rise to two separately labeled univalents (achiasmatic) chromosomes. To investigate this, chromosome-specific probes were labeled and used in FISH experiments. We found, as expected, that the chromosome-specific probes

(19, 17, 12, 2, 1, and X) labeled single individual chromosome structures in wild-type oocytes (Fig. 6, A–D). In contrast, FISH analysis identified a large number of $Sycp3^{-/-}$ oocytes that contained univalent chromosomes (Fig. 6, E–H, and Table II). The incidence of univalency for each of the six different meiotic

Table I. $Sycp3^{-/-}$ oocytes display variable γH2AX staining and different numbers of DMC1/RAD51 and MLH1 foci

$Sycp3^{-/-}$ oocytes	L pachytene/ E diplotene ($n_a = 103$; $n_b = 20$)	L diplotene ($n_a = 114$; $n_b = 38$; $n_c = 42$)	VL diplotene ($n_b = 41$; $n_c = 24$)
γH2AX	74% stronger 26% weaker	71% stronger 29% weaker	
DMC1/RAD51	80% foci >20 20% foci <20	71% foci >10 29% foci (0–10)	66% foci >5 34% foci (0–5)
MLH1		71% foci >15 29% foci (0–15)	67% foci >5[a] 33% foci (0–5)

$Sycp3^{-/-}$ oocytes were classified in groups depending on their level of γH2AX staining or the number of DMC1/RAD51 and MLH1 foci (n_a, counted oocytes for γH2AX; n_b, counted oocytes for DMC1/RAD51; and n_c, counted oocytes for MLH1) and shown as a relative percentage. E, early; L, late; VL, very late.
[a]These oocytes (except for one cell) also showed a stronger γH2AX staining pattern by coimmunostaining with MLH1 (Fig. 6).
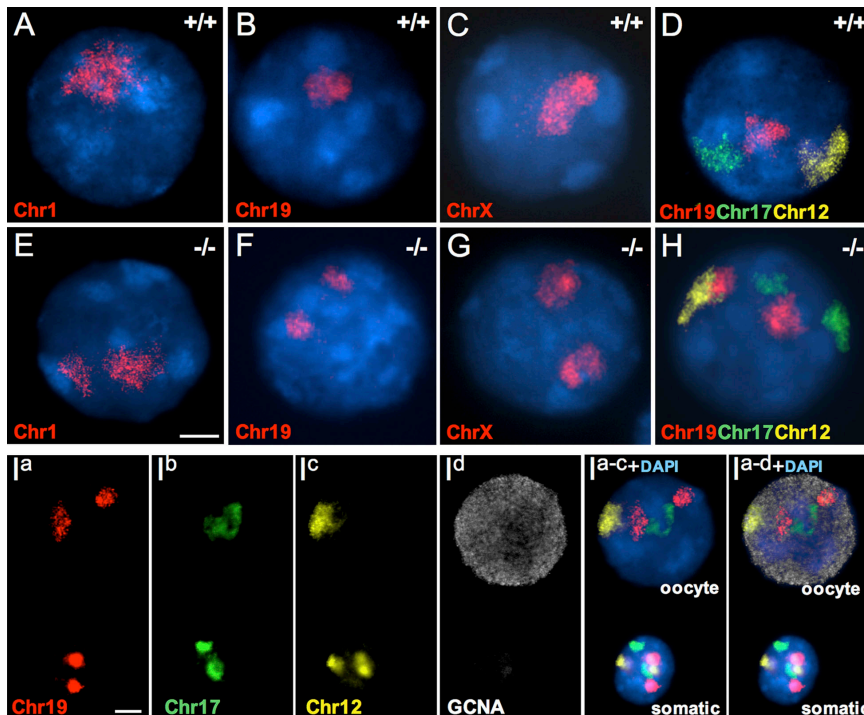
Figure 6. **Sycp3⁻/⁻ oocytes frequently contain univalent chromosomes as detected by FISH.** A single integral chromosome structure was detected by single- or triple-chromosome paints, as shown for Chr1 (A), Chr19 (B), ChrX (C), and Chr19 (red) + Chr17 (green) + Chr12 (yellow; D), in wild-type oocytes at 2 dpp. In contrast, two separately labeled univalent (achiasmatic) chromosomes were frequently detected in *Sycp3⁻/⁻* oocytes at 2 dpp, as visualized by the distinctly separated FISH signals shown for Chr1 (E), Chr19 (F), and ChrX (G). (H) Triple chromosome painting of a *Sycp3⁻/⁻* oocyte shows two signals for Chr19 (red), two signals for Chr17 (green), and one signal for Chr12 (yellow). (I) Oocytes were distinguished from ovarian somatic cells based on cell size and positive staining for the germ cell–specific marker GCNA. Bars, 10 μm.

chromosomes analyzed in *Sycp3⁻/⁻* oocytes at 2 dpp varied considerably (Table II). The difference in univalency rate for the six different chromosomes in the analyzed mutant mouse oocytes is best explained in the context of their reported mean chiasmata frequency (Hulten et al., 1995; Lawrie et al., 1995; Broman et al., 2002). Chromosomes 1 and 2 display an almost twofold higher mean chiasmata frequency than reported for chromosomes 12, 17, and 19, strongly suggesting that homologous chromosomes connected with two or more chiasmata are more likely to retain at least one chiasma even in the absence of SYCP3. Analysis of mutant oocytes using two or three chromosome-specific FISH probes simultaneously showed that many *Sycp3⁻/⁻* oocytes contain multiple univalent chromosomes (Table II). We conclude that the reduced efficiency of the DSB repair process in *Sycp3⁻/⁻* oocytes give rise to achiasmatic chromosomes and results in a sharp increase in the number of oocytes that contain univalent chromosomes at 2 dpp.

Oocytes containing univalent chromosomes are preferentially eliminated during early postnatal development

To follow the fate of the mutant oocytes during follicle formation, we studied the same six chromosomes in oocytes derived from females at 8 dpp by using FISH (Table II). We found that the percentage of mutant oocytes at 8 dpp that contained univalents for the analyzed chromosomes was reduced considerably compared with 2 dpp. For example, the percentage of oocytes having a univalent chromosome 19 at 2 dpp was reduced from 13 to ~6% at 8 dpp. Based on the reduced number of oocytes at 8 dpp in the *Sycp3⁻/⁻* ovary, our results suggest that oocytes that contain univalent chromosomes are preferentially eliminated during postnatal development. Using the combined statistics derived for the six chromosomes analyzed in Table II, we esti-

mate that although ~36% of the oocytes at 8 dpp retain univalent chromosomes, ~75% of the oocytes at 2 dpp contain univalent chromosomes. Our results therefore show that more than half of the oocytes that contain univalent chromosomes at 2 dpp are eliminated as the germ cell cysts mature into primordial follicles.

Discussion

Absence of SYCP3 reduces the efficiency of the meiotic DNA DSB repair process and affects crossover formation

It has been proposed that structural changes in the organization of the axial cores of meiotic chromosomes could affect the maturation of DSBs into crossovers (Blat et al., 2002). We show that loss of SYCP3 impairs both the DNA DSB repair process and the formation of crossovers between homologous chromosomes. The time course and nuclear distribution of phosphorylated H2AX and several recombination-related proteins were monitored during meiosis in *Sycp3⁻/⁻* oocytes. We found that several aspects of meiotic progression were not affected in *Sycp3⁻/⁻* oocytes, including the temporal appearance of γH2AX, the recruitment of RAD51/DMC1, RPA, MSH4, and MLH1 to DNA DSBs, or the time course of meiotic markers such as STAG3, SYCP1, and CREST. In contrast, we found that the removal of the phosphorylated form of H2AX was severely delayed in *Sycp3⁻/⁻* oocytes. Similarly, RAD51/DMC1, RPA, MSH4, and MLH1 foci persisted for an extended time period at the late meiotic stages in the mutant oocytes. Such patterns were not observed in wild-type oocytes and likely reflect a failure to complete recombination within the temporal window provided by meiotic prophase I. In agreement with this, we found that ~75% of the *Sycp3⁻/⁻* oocytes contain univalents

Table II. *Sycp3*^{−/−} oocytes that contain univalent chromosomes are preferentially eliminated during early postnatal development

Chromosome	2 dpp WT		2 dpp *Sycp3*^{−/−}		8 dpp WT		8 dpp *Sycp3*^{−/−}	
	Univalents/Total	%	Univalents/Total	%	Univalents/Total	%	Univalents/Total	%
ChrX	22/1,554	1.42	238/1,672	14.23	1/529	0.19	55/591	9.31
Chr1	13/1,025	1.27	11/350	3.14	2/888	0.23	2/304	0.66
Chr2	7/642	1.09	10/312	3.21	1/607	0.20	2/348	0.60
Chr12	22/1,865	1.18	113/1,350	8.37	3/1,240	0.24	15/808	1.86
Chr17	18/1,540	1.17	126/1,443	8.66	7/1,625	0.43	23/777	2.96
Chr19	23/1,939	1.19	191/1,414	13.51	5/1,339	0.37	48/857	5.60
Chr12 + 19	1/1,093	0.09	17/444	3.83	0/569	0.00	2/651	0.31
Chr17 + 19	0/930	0.00	17/517	3.29	0/723	0.00	2/666	0.30
Chr12 + 17	0/496	0.00	9/439	2.05	0/569	0.00	1/651	0.15
Chr12 + 17 + 19	0/496	0.00	5/439	1.14	0/569	0.00	0/651	0.00
ChrX + 19	0/338	0.00	11/251	4.38	0/187	0.00	2/142	1.42
ChrX + 17	2/338	0.59	11/251	4.38	0/187	0.00	2/184	1.09
ChrX + 17 + 19	0/338	0.00	4/251	1.59	0/187	0.00	0/142	0.00

Six individual chromosomes, and combinations of either two or three of these chromosomes, were analyzed by immunofluorescence FISH, and single or double FISH signals were scored. The number of oocytes that contained univalent chromosomes (separated FISH signals) versus the total numbers of oocytes was determined and the percentage of univalency was calculated for each analyzed chromosome. A similar analysis was done for oocytes derived from wild-type (WT) and *Sycp3*^{−/−} oocytes at postnatal days 2 and 8. The total number of univalent oocytes in the *Sycp3*^{−/−} ovary at 2 and 8 dpp was estimated as follows. A strong correlation exists between genetic chromosome length and chiasmata frequency (Lawrie et al., 1995). We found that the univalency rate for the chromosomes analyzed in this table followed this correlation, to a large extent. Therefore, we assumed that the average univalency rate affecting chromosomes 1–18 in *Sycp3*^{−/−} oocytes was 6% (the average observed for chromosomes 1, 2, 12, and 17). The univalency rates for chromosomes 19 and X were significantly higher compared to chromosomes 1–18 and, therefore, was added separately. A summary of the estimated univalency for all 20 chromosomes that was calculated as described above produced an outcome of 135%. However, as shown in Table II, many *Sycp3*^{−/−} oocytes contain multiple univalent chromosomes. We estimated this redundancy factor for all 20 chromosomes to affect 44% of the oocytes. (Whereas 45% of the oocytes analyzed for chromosomes 12, 17, 19, and X displayed univalency for one of the measured chromosomes, 20% of the oocytes analyzed using chromosomes 12, 17, 19, and X contained multiple univalent chromosomes. By dividing the 20% by 45%, we got a percentage of 44.) Therefore, the percentage of *Sycp3*^{−/−} oocytes affected by univalency should amount to ∼75% (1.35 × [1 − 0.44]). A similar calculation used to estimate the percentage of univalent cells at 8 dpp in *Sycp3*^{−/−} oocytes suggests that 36% of them contain achiasmatic chromosomes. The latter figure is in close agreement with the estimated aneuploidy rate observed for *Sycp3*^{−/−} females (Yuan et al., 2002).

at 2 dpp. It has been shown that the inactivation of proteins that participate in the repair of meiotic DNA DSBs activates a DNA damage checkpoint during early postnatal development, resulting in the complete elimination of affected oocytes (Di Giacomo et al., 2005). In agreement with this, we found that a majority of the *Sycp3*^{−/−} oocytes are eliminated beginning at 2 dpp. Furthermore, the increased loss of oocytes with univalent chromosomes during early postnatal development suggests that oocytes with incompletely repaired DNA are preferentially eliminated in *Sycp3*^{−/−} females. Together, these results suggest that the absence of SYCP3 activates a DNA damage checkpoint in oocytes.

The delayed removal of MLH1 foci in very late diplotene oocytes also provides an explanation to a previously contradictory observation in *Sycp3*^{−/−} oocytes (Yuan et al., 2002). It was shown that although the number of MLH1 foci at the pachytene stage in wild-type and *Sycp3*^{−/−} oocytes were approximately the same (Fig. 5 Q), the number of chiasmata at the MI stage was reduced in *Sycp3*^{−/−} oocytes compared with wild-type oocytes. Loss of MLH1 from meiotic chromosomes in wild-type meiotic cells normally precedes the removal of the SYCP1 protein, suggesting that the crossing-over process is completed in the context of an intact SC (Anderson et al., 1999; Moens et al., 2002). We found that some of the persistent MLH1 foci in very late diplotene *Sycp3*^{−/−} oocytes do not colocalize with residual SYCP1 staining. We propose that the uncoupling of the recombination process from synapsis in *Sycp3*^{−/−} oocytes affects the efficiency of the remaining MLH1 recombination

complexes and that a subset of these fails to complete the crossing-over process.

A failure to establish chiasmata between homologous chromosomes could also be caused by an impaired positive genetic-interference mechanism (Jones, 1984; Novak et al., 2001). This mechanism ensures that crossovers are correctly distributed between chromosomes. A partially inactivated interference mechanism could lead to an unregulated distribution of a fixed number of chiasmata and result in a loss of obligatory chiasmata, thereby generating achiasmatic chromosomes. It has been proposed that the SC ensures a high level of interference (Zickler, 1999; Nabeshima et al., 2004, MacQueen et al., 2005; Carlton et. al., 2006). We have studied if SYCP3 is required for interference by monitoring the number of MLH1 foci, which is a cytological marker for chiasmata distribution along SYCP1-labeled meiotic chromosomes (Baker et al., 1996; Edelmann et al., 1996; Hunter and Borts, 1997; Anderson et al., 1999). *Sycp3* deficiency increases the length of the meiotic chromosome axes by twofold and introduces irregular gaps in SYCP1 staining along the axes (the meiotic axis in the SYCP1-negative gaps cannot be traced with certainty, as antisera against cohesin complex proteins such as STAG3 only weakly stain these regions; Yuan et al., 2002; Kouznetsova et al., 2005). Therefore, it is impossible, using only cytological markers, to determine if individual meiotic chromosomes in *Sycp3*^{−/−} oocytes lack associated MLH1 foci. Instead, we selected *Sycp3*^{−/−} pachytene oocytes that displayed relatively intact SYCP1-labeled meiotic chromosomes and monitored the frequency of such structures,

which had two MLH foci associated to them. Analysis of 24 *Sycp3*$^{-/-}$ oocytes and 31 wild-type oocytes produced a very similar result, where both groups showed an average of ~3.5 intact SYCP1-labeled structures each having two MLH1 foci per cell. This result, therefore, does not support a model where the loss of SYCP3 negatively influences the impact of positive genetic interference in *Sycp3*$^{-/-}$ oocytes. It is important to note that in cases in *Sycp3*$^{-/-}$ oocytes where the TF structure as labeled by SYCP1 is severely fragmented, making it impossible to trace the meiotic chromosome axis, we cannot analyze if the MLH1 distribution pattern is affected. However, we only rarely identify entirely asynapsed homologous chromosomes (FISH studies suggest that ~1–2% of the pachytene *Sycp3*$^{-/-}$ oocytes contain asynapsed configurations of chromosome 19; unpublished data), excluding this as an important mechanism to explain the univalency statistics observed at 2 dpp in mutant oocytes.

Absence of SYCP3 generates oocytes with different levels of DNA damage, a subset of which evades two meiotic checkpoints

Our experiments show that loss of SYCP3 affects the efficiency of the DNA repair/recombination process. However, in contrast to the situation in mouse models, where components of the repair machinery have been inactivated (Di Giacomo et al., 2005), the repair/recombination process in *Sycp3*$^{-/-}$ oocytes is impaired, not blocked. We provide two sets of evidence for this; we found that ~34% of the oocyte pool remains at 8 dpp and of those that remain only approximately one-third contain univalent chromosomes. We also found a large diversity in the γH2AX staining pattern and the number of foci corresponding to RAD51/DMC1 and MLH1 in individual *Sycp3*$^{-/-}$ oocytes, strongly suggesting that loss of SYCP3 generates a temporal spectrum of recombination intermediates.

A fascinating aspect of the *Sycp3*$^{-/-}$ mouse model is the effectiveness with which it contributes to the formation of aneuploid offspring (Yuan et al., 2002). We have shown that *Sycp3*$^{-/-}$ oocytes that contain univalent chromosomes can bypass the DNA damage checkpoint at early postnatal development. A similar situation has been noted in mice that are deficient for MLH1 (Baker et al., 1996; Edelman et al., 1996). In these mice the final crossovers are not completed, giving rise to the formation of achiasmatic chromosomes; however, the DNA damage checkpoint does not become activated. In sharp contrast to *Mlh*-deficient oocytes (Woods et al., 1999), however, *Sycp3*-deficient oocytes that contain univalent chromosomes also bypass the spindle checkpoint at the first meiotic cell division and give rise to aneuploid offspring (Yuan et al., 2002). Our results for *Sycp3*-deficient oocytes are in agreement with studies of human oocytes that suggest that a reduced level of recombination is linked to an increase in aneuploidy (Hassold and Hunt, 2001). Interestingly, it has been observed that γH2AX signals are more slowly removed during meiosis in human oocytes compared with sperm, suggesting that progression of DSB repair is slower in oocytes (Roig et al., 2004).

We have shown that loss of *Sycp3*$^{-/-}$ oocytes does not occur until the diplotene stage. In contrast, *Sycp3*$^{-/-}$ spermatocytes are already eliminated at the zygotene/pachytene stage of meiosis (Yuan et al., 2000). A similar temporal difference in the loss of damaged male and female germ cells has been noted for a large number of gene deficiencies (Hunt and Hassold, 2002). We propose that the relative incidence of aneuploidy observed for male and female gametes can be partly explained by a temporal difference in the activation of the DNA damage checkpoint during meiosis. In cases where a mutation generates a temporal spectrum of recombination deficiencies, the timing of the activation of the DNA damage checkpoint becomes crucial. The late activation of the female DNA damage checkpoint during meiosis, relative to the temporal activation of the same checkpoint in male germ cells, provides additional time for the formation of advanced recombination intermediates that can no longer be detected by this checkpoint in oocytes. This increases the risk that such recombination intermediates will contribute to the formation of univalent chromosomes.

Materials and methods

Generation of *Sycp3*$^{-/-}$ mice

Derivation of the *Sycp3* knockout mice has been previously described (Yuan et al., 2000). In brief, C57BL/6NCrkBR wild-type males were mated with *Sycp3*$^{-/-}$ females to generate *Sycp3*$^{+/-}$ offspring. Nonsibling *Sycp3*$^{+/-}$ males and females were then mated to produce *Sycp3*$^{+/+}$ (wild-type) and *Sycp3*$^{-/-}$ mice. To detect the pregnancy, two females were caged with one male after 16:00 (4:00 pm). The vaginal plugs were examined daily between 8:00 and 9:00 (am). The day that the plug was found was defined as E0.5. For ovary collection at embryonic stages, pregnant mice were killed at E16.5, E17.5, and E18.5. For ovary collection at postnatal stages, the pups were killed after birth at days 1, 2, 4, and 8, which were referred to as 1, 2, 4, and 8 dpp. Ovaries from adult mice were also collected at 8 wk.

Histomorphometry

Ovaries were fixed in 4% paraformaldehyde for 4 h before paraffin embedding. The entire ovary embedded in the paraffin was sequentially sectioned at 5 μm. Every tenth section was stained either by hematoxylin and eosin or immunostained for GCNA, which is a germ cell marker (Enders and May, 1994), or c-kit, which is an oocyte marker (Manova et al., 1990). These sections were then used for estimation of oocyte numbers. In embryonic and newborn ovaries, oocytes can be clearly distinguished from somatic cells by GCNA staining. Immunohistochemistry was performed with a rat anti–GCNA-1 (a gift from G.C. Enders, University of Kansas Medical Center, Kansas City, KS) and a polyclonal rabbit anti–c-kit (PC34; Oncogene Research Products), using the Vectastain Elite ABC kit (SK 4100; Vector Laboratories), according to the manufacturer's instructions. The peroxidase substrate DAB (DakoCytomation) was used to visualize the immunostaining reaction and hematoxylin was used for counterstaining. For the postnatal mice ovaries, primordial and primary follicles were defined by their morphology and by c-kit immunostaining. Oocyte counts were first determined individually for germ cell cysts (germ cells that were not individually separated by stromal cells), primordial follicles (small oocytes surrounded by a few flattened pregranulosa cells), primary follicles (oocytes with a visible nucleolus surrounded by a single layer of cuboidal granulosa cells, ranging from five to nine cells), and secondary follicles (an oocyte with a visible nucleolus surrounded by two layers of cuboidal granulosa cells made up of more than eight granulosa cells). Only follicles with a visible nucleus were counted to avoid double counting. The total oocyte numbers for each ovary were summarized from different follicle stages by using five sections/ovary (6 sections/ovary in 8-dpp mice and 15 sections/ovary in 8 wk-old mice). Three to seven ovaries per genotype (null and wild-type mice were from the same litter) were included in each group.

TUNEL assay

Apoptotic cells in paraffin-embedded sections of ovaries were identified using a TUNEL staining kit (Seriologicals Corp.), following the manufacturer's instructions. The sections were counterstained with methyl green. Every tenth section from the same ovary used for oocyte counting was also used for TUNEL staining. The relative number of apoptotic cell was summarized

from five sections/ovary for each study group, with the exception of six sections taken from ovaries derived from 8-dpp mice.

Statistics
Statistical calculations of oocyte numbers were performed by one-way analysis of variance, using the SigmaStat program (SPSS, Inc.). $P \leq 0.05$ indicates a significant difference.

Immunofluorescence microscopy
Wild-type and $Sycp3^{-/-}$ oocytes were obtained using a "dry-down" technique (Peters et al., 1997) from ovaries at E16.5 (early and later zygotene oocyte), E18.5, and E19.5 (pachytene and diplotene oocytes). RAD51/DMC1, RPA, and MSH4 foci counting was performed at five different meiotic stages in wild-type and $Sycp3^{-/-}$ oocytes. Staging of oocytes was performed using several markers, including SYCP1, STAG3, and CREST, as well as DAPI (Fig. S2; Kouznetsova et al., 2005). In early zygotene, synapsis has started and short SYCP1 fibers are visible, but centromeres are not yet paired (around 40 CREST foci). In zygotene, up to 50% of the AEs take part in synapsis and centromere pairing has been initiated. In late zygotene, 50–80% of the AEs take part in synapsis and most centromeres are paired (generating ~20 CREST foci). In late pachytene and early diplotene, a majority of the AEs are synapsed, and if some bivalents have desynapsed they appear to repel each other; most centromeres are still paired. In late diplotene, most of the SYCP1 fibers have disappeared, and the number of CREST foci varies between 20 and 40. Mutant oocytes were assigned a stage when the aforementioned criteria were fulfilled. Primary antibodies and dilutions used were guinea pig anti-SYCP1 and anti-STAG3 at 1:200 (Kouznetsova et al., 2005), human anti-CREST at 1:1,000, mouse anti-γH2AX (Upstate Biotechnology) at 1:100, rabbit anti-DMC1/RAD51 at 1:100 and rabbit anti-RPA at 1:500 (gifts from P. Moens, York University, Toronto, Canada), rabbit anti–human MSH4 (a gift from C. Her, Washington State University, Pullman, WA) at 1:100, and mouse anti–human MLH1 (BD Biosciences). All primary antibody incubations were performed overnight at 4°C or 37°C. Secondary antibodies were swine anti–rabbit conjugated to FITC (DakoCytomation) at 1:100, donkey anti–guinea pig conjugated to Cy3 (Jackson ImmunoResearch Laboratories) at 1:1,000, goat anti–human conjugated to Cy5 (GE Healthcare), goat anti–mouse Alexa Fluor 488 (Invitrogen) at 1:1,000, and goat anti–rabbit Alexa Fluor 350 (Invitrogen) at 1:500. All secondary antibodies were incubated for 1 h at room temperature. DNA was stained with DAPI. Slides were mounted with antifade medium before being analyzed. Slides were viewed at room temperature using fluorescence microscopes (DMRA2 and DMRXA; Leica) and 100× objectives (Leica) with an aperture of 1.4 providing epifluorescence. Images were captured with a digital charge-coupled device camera (model C4742-95; Hamamatsu) and the Openlab 3.1.4 software (Improvision). Images were processed using Photoshop version 9 (Adobe).

Identification of univalent chromosomes by immunofluorescence FISH
Oocytes were obtained from 2- and 8-dpp female mice ovaries. To increase the yields of oocytes from 8-dpp mice, ovaries were initially incubated for 30 min at 37°C with collagenase and DNase (Eppig, 1994). The cells were isolated by pipetting and fixed by using 1% paraformaldehyde and 0.15% Triton X-100. Oocytes were detected by GCNA staining. The oocytes were also distinguished from somatic cells on the basis of their size, the dispersed nature of their chromatin, and a characteristic congregation of centromeres at several distinct locations within the nucleus (Hodges et al., 2001). After immunostaining, the slides were washed and air dried, and then denatured in 70% formamide and 2× SSC at 70°C for 2–4 min. Hybridization with specific chromosome probes was performed for 40 h at 37°C. The Cy3-labeled chromosomal probes (Chrombios GmbH) were used to identify chromosomes 1, 2, 12, 17, 19, and X in the oocyte by using FISH. Double- and triple-color FISH probes were labeled with Chr19-Cy3, Chr17-Cy5, and Chr12 (or ChrX)-DEAC. The washing step followed the manufacturer's protocols (Chrombios GmbH). DAPI was used as a DNA counterstain, and slides were mounted with antifade before analysis.

Online supplemental material
Fig. S1 shows that an increased number of oocytes are TUNEL positive in the $Sycp3^{-/-}$ ovary. Fig. S2 shows the classification of zygotene and diplotene stage meiotic cells. Online supplemental material is available at http://www.jcb.org/cgi/content/full/jcb.200512077/DC1.

References

Alani, E., R. Thresher, J.D. Griffith, and R.D. Kolodner. 1992. Characterization of DNA-binding and strand-exchange stimulation properties of y-RPA, a yeast single-strand-DNA-binding protein. *J. Mol. Biol.* 227:54–71.

Anderson, L.K., A. Reeves, L.M. Webb, and T. Ashley. 1999. Distribution of crossing over on mouse synaptonemal complexes using immunofluorescent localization of MLH1 protein. *Genetics.* 151:1569–1579.

Baker, S.M., A.W. Plug, T.A. Prolla, C.E. Bronner, A.C. Harris, X. Yao, D.M. Christie, C. Monell, N. Arnheim, A. Bradley, et al. 1996. Involvement of mouse Mlh1 in DNA mismatch repair and meiotic crossing over. *Nat. Genet.* 13:336–342.

Blat, Y., R.U. Protacio, N. Hunter, and N. Kleckner. 2002. Physical and functional interactions among basic chromosome organizational features govern early steps of meiotic chiasma formation. *Cell.* 111:791–802.

Broman, K.W., L.B. Rowe, G.A. Churchill, and K. Paigen. 2002. Crossover interference in the mouse. *Genetics.* 160:1123–1131.

Carlton, P.M., A.P. Farruggio, and A.F. Dernburg. 2006. A link between meiotic prophase progression and crossover control. *PLoS Genet.* 2:e12.

Celeste, A., S. Petersen, P.J. Romanienko, O. Fernandez-Capetillo, H.T. Chen, O.A. Sedelnikova, B. Reina-San-Martin, V. Coppola, E. Meffre, M.J. Difilippantonio, et al. 2002. Genomic instability in mice lacking histone H2AX. *Science.* 296:922–927.

de Vries, F.A., E. de Boer, M. van den Bosch, W.M. Baarends, M. Ooms, L. Yuan, J.G. Liu, A.A. van Zeeland, C. Heyting, and A. Pastink. 2005. Mouse Sycp1 functions in synaptonemal complex assembly, meiotic recombination, and XY body formation. *Genes Dev.* 19:1376–1389.

Di Giacomo, M., M. Barchi, F. Baudat, W. Edelmann, S. Keeney, and M. Jasin. 2005. Distinct DNA-damage-dependent and -independent responses drive the loss of oocytes in recombination-defective mouse mutants. *Proc. Natl. Acad. Sci. USA.* 102:737–742.

Dobson, M.J., R.E. Pearlman, A. Karaiskakis, B. Spyropoulos, and P.B. Moens. 1994. Synaptonemal complex proteins: occurrence, epitope mapping and chromosome disjunction. *J. Cell Sci.* 107(Pt 10):2749–2760.

Edelmann, W., P.E. Cohen, M. Kane, K. Lau, B. Morrow, S. Bennett, A. Umar, T. Kunkel, G. Cattoretti, R. Chaganti, et al. 1996. Meiotic pachytene arrest in MLH1-deficient mice. *Cell.* 85:1125–1134.

Enders, G.C., and J.J. May II. 1994. Developmentally regulated expression of a mouse germ cell nuclear antigen examined from embryonic day 11 to adult in male and female mice. *Dev. Biol.* 163:331–340.

Eppig, J.J. 1994. Further reflections on culture systems for the growth of oocytes in vitro. *Hum. Reprod.* 9:974–976.

Gerton, J.L., and R.S. Hawley. 2005. Homologous chromosome interactions in meiosis: diversity amidst conservation. *Nat. Rev. Genet.* 6:477–487.

Hassold, T., and P. Hunt. 2001. To err (meiotically) is human: the genesis of human aneuploidy. *Nat. Rev. Genet.* 2:280–291.

Hodges, C.A., R. LeMaire-Adkins, and P.A. Hunt. 2001. Coordinating the segregation of sister chromatids during the first meiotic division: evidence for sexual dimorphism. *J. Cell Sci.* 114:2417–2426.

Hulten, M.A., C. Tease, and N.M. Lawrie. 1995. Chiasma-based genetic map of the mouse X chromosome. *Chromosoma.* 104:223–227.

Hunt, P.A., and T.J. Hassold. 2002. Sex matters in meiosis. *Science.* 296:2181–2183.

Hunter, N., and R.H. Borts. 1997. Mlh1 is unique among mismatch repair proteins in its ability to promote crossing-over during meiosis. *Genes Dev.* 11:1573–1582.

Jones, G.H. 1984. The control of chiasma distribution. *Symp. Soc. Exp. Biol.* 38:293–320.

Kouznetsova, A., I. Novak, R. Jessberger, and C. Hoog. 2005. SYCP2 and SYCP3 are required for cohesin core integrity at diplotene but not for centromere cohesion at the first meiotic division. *J. Cell Sci.* 118:2271–2278.

Lammers, J.H., H.H. Offenberg, M. van Aalderen, A.C. Vink, A.J. Dietrich, and C. Heyting. 1994. The gene encoding a major component of the lateral elements of synaptonemal complexes of the rat is related to X-linked lymphocyte-regulated genes. *Mol. Cell. Biol.* 14:1137–1146.

Lawrie, N.M., C. Tease, and M.A. Hulten. 1995. Chiasma frequency, distribution and interference maps of mouse autosomes. *Chromosoma.* 104:308–314.

Lydall, D., Y. Nikolsky, D.K. Bishop, and T. Weinert. 1996. A meiotic recombination checkpoint controlled by mitotic checkpoint genes. *Nature*. 383:840–843.

Lynn, A., K.E. Koehler, L. Judis, E.R. Chan, J.P. Cherry, S. Schwartz, A. Seftel, P.A. Hunt, and T.J. Hassold. 2002. Covariation of synaptonemal complex length and mammalian meiotic exchange rates. *Science*. 296:2222–2225.

MacQueen, A.J., C.M. Phillips, N. Bhalla, P. Weiser, A.M. Villeneuve, and A.F. Dernburg. 2005. Chromosome sites play dual roles to establish homologous synapsis during meiosis in C. elegans. *Cell*. 123:1037–1050.

Mahadevaiah, S.K., J.M. Turner, F. Baudat, E.P. Rogakou, P. de Boer, J. Blanco-Rodriguez, M. Jasin, S. Keeney, W.M. Bonner, and P.S. Burgoyne. 2001. Recombinational DNA double-strand breaks in mice precede synapsis. *Nat. Genet.* 27:271–276.

Manova, K., K. Nocka, P. Besmer, and R.F. Bachvarova. 1990. Gonadal expression of c-kit encoded at the W locus of the mouse. *Development*. 110:1057–1069.

Marcon, E., and P.B. Moens. 2005. The evolution of meiosis: recruitment and modification of somatic DNA-repair proteins. *Bioessays*. 27:795–808.

Moens, P.B., N.K. Kolas, M. Tarsounas, E. Marcon, P.E. Cohen, and B. Spyropoulos. 2002. The time course and chromosomal localization of recombination-related proteins at meiosis in the mouse are compatible with models that can resolve the early DNA-DNA interactions without reciprocal recombination. *J. Cell Sci.* 115:1611–1622.

Nabeshima, K., A.M. Villeneuve, and K.J. Hillers. 2004. Chromosome-wide regulation of meiotic crossover formation in Caenorhabditis elegans requires properly assembled chromosome axes. *Genetics*. 168:1275–1292.

Neyton, S., F. Lespinasse, P.B. Moens, R. Paul, P. Gaudray, V. Paquis-Flucklinger, and S. Santucci-Darmanin. 2004. Association between MSH4 (MutS homologue 4) and the DNA strand-exchange RAD51 and DMC1 proteins during mammalian meiosis. *Mol. Hum. Reprod.* 10:917–924.

Novak, J.E., P.B. Ross-Macdonald, and G.S. Roeder. 2001. The budding yeast Msh4 protein functions in chromosome synapsis and the regulation of crossover distribution. *Genetics*. 158:1013–1025.

Page, S.L., and R.S. Hawley. 2004. The genetics and molecular biology of the synaptonemal complex. *Annu. Rev. Cell Dev. Biol.* 20:525–558.

Peters, A.H., A.W. Plug, M.J. van Vugt, and P. de Boer. 1997. A drying-down technique for the spreading of mammalian meiocytes from the male and female germline. *Chromosome Res.* 5:66–68.

Petronczki, M., M.F. Siomos, and K. Nasmyth. 2003. Un menage a quatre: the molecular biology of chromosome segregation in meiosis. *Cell*. 112:423–440.

Rajkovic, A., S.A. Pangas, D. Ballow, N. Suzumori, and M.M. Matzuk. 2004. NOBOX deficiency disrupts early folliculogenesis and oocyte-specific gene expression. *Science*. 305:1157–1159.

Roeder, G.S., and J.M. Bailis. 2000. The pachytene checkpoint. *Trends Genet.* 16:395–403.

Roig, I., B. Liebe, J. Egozcue, L. Cabero, M. Garcia, and H. Scherthan. 2004. Female-specific features of recombinational double-stranded DNA repair in relation to synapsis and telomere dynamics in human oocytes. *Chromosoma*. 113:22–33.

Schalk, J.A., A.J. Dietrich, A.C. Vink, H.H. Offenberg, M. van Aalderen, and C. Heyting. 1998. Localization of SCP2 and SCP3 protein molecules within synaptonemal complexes of the rat. *Chromosoma*. 107:540–548.

Shinohara, A., and M. Shinohara. 2004. Roles of RecA homologues Rad51 and Dmc1 during meiotic recombination. *Cytogenet. Genome Res.* 107:201–207.

Turner, J.M., S.K. Mahadevaiah, O. Fernandez-Capetillo, A. Nussenzweig, X. Xu, C.X. Deng, and P.S. Burgoyne. 2005. Silencing of unsynapsed meiotic chromosomes in the mouse. *Nat. Genet.* 37:41–47.

Wang, X., and J.E. Haber. 2004. Role of *Saccharomyces* single-stranded DNA-binding protein RPA in the strand invasion step of double-strand break repair. *PLoS Biol.* 2:E21.

Woods, L.M., C.A. Hodges, E. Baart, S.M. Baker, M. Liskay, and P.A. Hunt. 1999. Chromosomal influence on meiotic spindle assembly: abnormal meiosis I in female Mlh1 mutant mice. *J. Cell Biol.* 145:1395–1406.

Yuan, L., J.G. Liu, J. Zhao, E. Brundell, B. Daneholt, and C. Hoog. 2000. The murine SCP3 gene is required for synaptonemal complex assembly, chromosome synapsis, and male fertility. *Mol. Cell*. 5:73–83.

Yuan, L., J.G. Liu, M.R. Hoja, J. Wilbertz, K. Nordqvist, and C. Hoog. 2002. Female germ cell aneuploidy and embryo death in mice lacking the meiosis-specific protein SCP3. *Science*. 296:1115–1118.

Zickler, D. 1999. The synaptonemal complex: a structure necessary for pairing, recombination or organization of the meiotic chromosome? *J. Soc. Biol.* 193:17–22.

Zickler, D., and N. Kleckner. 1999. Meiotic chromosomes: integrating structure and function. *Annu. Rev. Genet.* 33:603–754.